Proton-induced reactions on ^{6}He at low energies

N. K. Timofeyuk and I. J. Thompson
University of Surrey, Guildford, Surrey GU2 5XH, United Kingdom
(Received 8 September 1999; published 15 March 2000)

Finite-range coupled channel calculations of proton-induced reactions on ^{6}He have been performed below the ^{6}He three-body breakup threshold, assuming that the α particle core is inert. The coupling scheme included all transitions between open channels and therefore no imaginary parts of the interaction potentials were used. The calculations have revealed a complicated dynamics of the $p+{}^6$He interaction at the chosen energy, with couplings to all open channels being important to generate the final cross sections. The total absorption from the elastic $p+{}^6$He channel depends on the details of the interactions employed in the three-body model of ^{6}He and shows a strong correlation with the r.m.s. radius of ^{6}He. The role of the exchange mechanisms was investigated within the framework of the distorted-wave Born approximation. It was found that both the triton exchange $^6\mathrm{He}(p,{}^4\mathrm{He})t$ and two-neutron $^6\mathrm{He}(p,t)^4\mathrm{He}$ direct transfer mechanisms produce comparable cross sections. The investigation of the radiative capture $^6\mathrm{He}(p,\gamma)^7\mathrm{Li}$ in the potential model shows strong suppression of the $E1$ transition because of the destructive interference between the external and internal contributions to the reaction amplitude and the absorption in the incident channel.

PACS number(s): 24.10.Eq, 25.40.−h, 25.60.−t, 27.20.+n

I. INTRODUCTION

Nuclear reactions induced by radioactive ^{6}He beams are considered as a source of our knowledge about the structure of the ^{6}He nucleus. However, since the information about the structure is obtained from such reactions indirectly, its accuracy depends strongly on the adequate description of the reaction dynamics. It is clear that the low three-body breakup threshold in ^{6}He creates difficulties for the theoretical interpretation of the experimental data. Other problems may arise due to the target excitations. To minimize the uncertainties caused by the reaction dynamics one can either significantly increase the incident energy of the ^{6}He beam so that only the simplest reaction mechanisms survive, or go below the ^{6}He breakup threshold and to use a hydrogen target.

In this paper we consider ^{6}He-induced reactions by a hydrogen target at very low energies. An experiment with 6 MeV ^{6}He beam on ^{12}C target has been already done at Louvain-la-Neuve cyclotron [1]. A peak from the $^6\mathrm{He}(p,t)^4\mathrm{He}$ reaction was also seen in this experiment due to the small hydrogen contamination of the target, which suggested large cross sections of this reaction. The corresponding center-of-mass energy of the proton in this case was 0.87 MeV. At such an energy the ^{6}He breakup channel is closed, which simplifies the theoretical interpretation of the reaction mechanism. On the other hand, since the Coulomb barrier for the $p+{}^6$He system is only about 400 keV, the protons could penetrate inside ^{6}He, thus providing us with information about the ^{6}He structure.

Only a few channels are open in the p-^{6}He scattering at $E_p^{\mathrm{c.m.}}=0.87$ MeV: charge exchange $^6\mathrm{He}(p,n)^6\mathrm{Li}_{0,1}$, one nucleon transfer $^6\mathrm{He}(p,d)^5\mathrm{He}$, two neutron transfer $^6\mathrm{He}(p,t)^4\mathrm{He}$, and radiative capture $^6\mathrm{He}(p,\gamma)^7\mathrm{Li}_{0,1}$. One would expect that all these reactions should result from the interaction of protons with valence neutrons of ^{6}He while the α core can be considered as inert. The charge exchange reactions (p,n) and (n,p) on $A=6$ target have been studied at higher energies in the four-body distorted wave theory earlier [2]. It was found that one can obtain a good description of the absolute values of the differential cross sections if the three-body nature of the ^{6}He nucleus is taken into account. The population of the ^{6}Li in the final state may proceed, however, via the two-step process $(p,d)(d,n)$ whose role at low energies is not clear. The same neutron transfer reaction (p,d) initiates the two-step $(p,d)(d,t)$ flux to the $^4\mathrm{He}+t$ channel. This two-step process competes with the direct two neutron transfer (p,t) which is believed to be a good test for two-body nucleon-nucleon correlations in atomic nuclei. Since the dominant component of the ^{6}He wave function is represented by a correlated dineutron pair moving around the α core [3], the transfer of the correlated dineutron pair may significantly influence the cross sections of the (p,t) reaction. The existing theoretical calculations of the $^6\mathrm{He}(p,t)^4\mathrm{He}$ reaction at $E_{\mathrm{lab}}=2-5$ MeV/nucleon [4] predict a strong competition between sequential and direct processes at low energies. However, these calculations underestimate the experimentally measured cross sections at $E_{\mathrm{lab}}=3.2$ MeV/nucleon in [5] by about three orders of magnitude. Recent studies of $^6\mathrm{He}(p,t)^4\mathrm{He}$ reaction at higher energy in [6] indicate that the transfer of the correlated dineutron makes the dominant contribution of the cross section of this reaction.

According to the general reaction theory, open channels give rise to imaginary parts in the interaction potentials. The imaginary parts are absent, however, if all the open channels are taken into account explicitly in the coupled-channel formalism. Since the number of the open channels in the p-^{6}He scattering is reasonably small, there exists an opportunity to perform the full coupled-reaction-channel (CRC) calculations between these channels with zero imaginary parts for all the projectile-target potentials involved.

In this paper, we consider all possible two-way couplings between the above-mentioned channels excluding the $^6\mathrm{He}(p,\gamma)^7\mathrm{Li}$ electromagnetic channel. We estimate the $^6\mathrm{He}(p,\gamma)^7\mathrm{Li}$ cross section separately in the direct radiative capture model. We investigate the sensitivity of the angular distributions of elastic scattering and all reactions to the re-

 ©2000 The American Physical Society

action dynamics considered, and to the choice of the three-body ^{6}He wave function.

In Sec. II the finite-range coupled channel calculations of the proton-induced reactions on ^{6}He are performed. In Sec. III we estimate the role of the exchange effects within the framework of the distorted-wave Born approximation (DWBA). In Sec. IV the contribution of the radiative capture $^6\mathrm{He}(p,\gamma)^7\mathrm{Li(g.s.)}$ is estimated. Some concluding remarks are given in Sec. V.

II. COUPLED CHANNELS IN THE LOW-ENERGY p-^{6}He SCATTERING

Strictly speaking, the p-^{6}He scattering is a seven-body problem. In the coupled reaction channel (CRC) formalism this seven-body dynamics is replaced by the coupling of N possible *pairs* of subclusters m_{1i} and m_{2i} in different partitions $i=1\ldots N$, where $m_{1i}+m_{2i}=7$. The total wave function is represented by a sum of product of pairs of internal ϕ_{1i} and ϕ_{2i} and relative F_i wave functions in the various partitions:

$$\Psi=\sum_{i=1}^{N}\phi_{1i}\phi_{2i}F_i(\vec{R}_i)/R_i, \tag{1}$$

where $\vec{R}_i$ is the relative coordinate between the two fragments in partition i.

The radial relative wave functions f_α are obtained from the solutions of radial Schrödinger equations for total energy E:

$$\left[-\frac{\hbar^2}{2\mu_i}\left(\frac{d^2}{dR_i^2}-\frac{L_\alpha(L_\alpha+1)}{R_i^2}\right)+\epsilon_{1i}+\epsilon_{2i}-E\right]f_\alpha(R_i)+\sum_{\alpha'}\int_0^{R_m}dR'\,V_{\alpha:\alpha'}(R_i,R')f_{\alpha'}(R')=0, \tag{2}$$

where α is a general index that includes i as well as the angular momentum quantum numbers. The R_m is the radius outside of which all couplings are assumed to be zero, and is taken as 50 fm in the present calculations. The nonlocal terms with $V_{\alpha:\alpha'}(R_i,R')$ arise from the transfer of one or more nucleons, coupling together the different partitions i and i', and may have *post* or *prior* forms that should be equivalent when the appropriate nonorthogonality terms are included. The energies ϵ_{1i} and ϵ_{2i} are the internal energies of nuclear states ϕ_{1i} and ϕ_{2i}, respectively, and μ_i is the reduced mass $m_{1i}m_{2i}/(m_{1i}+m_{2i})$. Equations (2) are solved iteratively using the code FRESCO [7], with Padé acceleration if necessary near resonances, as described in Ref. [7].

In the case of $p+{}^6$He the following partitions can be considered below the breakup threshold:

I $p+{}^6\mathrm{He}(0^+,\mathrm{g.s.})$,

II $d+{}^5\mathrm{He}(3/2^-)$,

IIIa $n+{}^6\mathrm{Li}(1^+,\mathrm{g.s.})$,

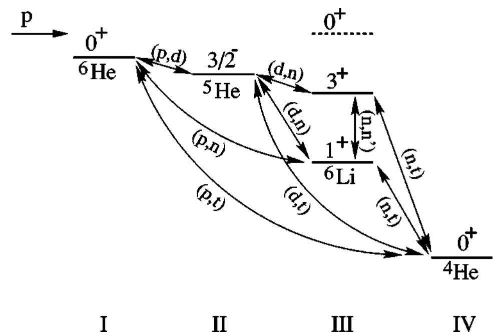

FIG. 1. Coupling scheme for the $p+{}^6$He scattering.

IIIb $n+{}^6\mathrm{Li}(3^+,2.18\ \mathrm{MeV})$,

IV $t+{}^4$He.

The coupling scheme between these partitions is presented in Fig. 1. If the proton center-of-mass energy is larger than 0.838 MeV, then an isobar-analog channel

IIIc $n+{}^6\mathrm{Li}(0^+,3.56\ \mathrm{MeV})$

is open as well. To minimize the number of channels we will consider the proton energies below this threshold. Actually, we make calculations at $E_p^{\mathrm{lab}}=0.97$ MeV which corresponds to the maximum energy of the ^{6}He beam at which the channel IIIc is closed. Let us note that at this energy the ^{6}He and deuteron breakup channels are closed. Although virtual breakup of the ^{6}He and/or the deuteron may take place, these are still included in the CRC formalism insofar as they are nonorthogonal to the rearrangement channels.

There exists also an open three-body channel $^4\mathrm{He}+d+n$ at the energy considered. This channel contains low-energy p-wave and d-wave resonances in the $^4\mathrm{He}+n$ and $\alpha+d$ subsystems. Therefore, one would expect that the population of these resonances would exhaust the major part of the $^4\mathrm{He}+d+n$ continuum. We describe the $^4\mathrm{He}+n$ and $^4\mathrm{He}+d$ resonances by the continuum bin wave functions (see Ref. [7]) calculated with the corresponding $^4\mathrm{He}+n$ and $^4\mathrm{He}+d$ potentials which provide correct locations of these resonances, and we present the $^4\mathrm{He}+d+n$ continuum as two-body $d+{}^5$He and $n+{}^6\mathrm{Li}(3^+)$ channels (partitions II and IIIb, respectively). The population of these two-body channels in the three-body continuum is explicitly treated in this paper.

In the following we will use two ^{6}He three-body wave functions to determine the $^4\mathrm{He}+n+n$ dynamics [3]. These are both calculated using the hyperspherical harmonic expansion method, and include hyperharmonics up to $K_{\max}=20$. The first (A), from [8], has a two-neutron separation energy of 0.975 MeV and, with an α particle rms matter radius of 1.49 fm, yields a ^{6}He rms matter radius of 2.50 fm. The second wave function (B), calculated assuming a modified three-body interaction term, has separation energy 0.985 MeV, and produces a ^{6}He nucleus with a smaller rms matter radius of 2.35 fm. Both use the n-^{4}He potential from Ref. [9], and the Gogny-Pires-Tourrell n-n potential [10] with spin-orbit and tensor components. A triton wave function was constructed with the same hyperspherical harmonic expansion method with $K_{\max}=28$. We fitted an additional scalar three-body potential to the experimental binding energy, and obtain a triton rms matter radius of 1.8 fm. The two-nucleon transfer form factors $\langle ^6\mathrm{He}|\alpha\rangle$ and $\langle p|t\rangle$ and the corresponding vertex functions $\langle ^6\mathrm{He}|V_{n_1\alpha}+V_{n_2\alpha}|\alpha\rangle$ and $\langle p|V_{n_1p}+V_{n_2p}|t\rangle$ were calculated from the three-body models for ^{6}He and triton using the same interactions in the transition operator that were used to calculate the wave functions. The A and B ^{6}He wave functions, both with the correct breakup threshold, will allow us to gain a first impression of the sensitivity of the low-energy reaction calculations to the assumed three-body wave function of ^{6}He. Preliminary corresponding predictions for Coulomb breakup have already been examined [11].

Since all the open channels are included in the coupling scheme, we set the imaginary parts of projectile-target potentials to zero and we represent their real parts by folding potentials. We calculate the folding potentials for partitions I, III, and IV using the M3Y effective interactions [12], that are based on the Reid-soft-core NN potential with a knockon exchange term. The ^{6}Li, ^{4}He, and triton densities were taken from the electron scattering [13], with Gaussian form, while the A and B ^{6}He densities for folding were derived from the corresponding three-body wave functions with a Gaussian α density of radius 1.49 fm given above. We calculate the d-$^5\mathrm{He}(3/2^-)$ potential by folding the d-n and d-^{4}He interactions with n-^{4}He continuum bin wave function that is found using the n-^{4}He potential again of Ref. [9]. The depths of the d-n and d-α potentials have been chosen to reproduce the triton and ^{6}Li(g.s.) bound states in the two-body potential model.

To calculate the $\langle ^6\mathrm{He}|^5\mathrm{He}\rangle$, $\langle ^6\mathrm{Li}|^5\mathrm{He}\rangle$, $\langle t|d\rangle$, $\langle p|d\rangle$, $\langle n|d\rangle$, and $\langle ^6\mathrm{Li(g.s.)}|^4\mathrm{He}\rangle$ overlap integrals, the well depth procedure was used[1] with standard geometry parameters $r_0=1.25$ fm and $a=0.65$ fm everywhere except for the ^{6}Li(g.s.) nucleus where $R=4^{1/3}r_0$, $r_0=1.575$ fm were used. For $^6\mathrm{Li}(3^+)$ the d-^{4}He model is used with $V=115.06$ MeV, $r_0=1.575$, and $a=0.65$ fm to reproduce the resonance in the d wave at 0.711 MeV. No spin-orbit potentials were used in these cases. All the spectroscopic amplitudes were consistently calculated within the translation-invariant shell-model [14] using shell-model wave functions from [15]. The values of these spectroscopic amplitude are given in Table I, where their signs have been changed according to FRESCO's convention for angular momentum couplings: $\vec{l}+\vec{s}_{1i}=\vec{j}$, $\vec{j}+\vec{s}_{2i}=\vec{J}$ with s_{1i} and s_{2i} being spins of subclusters 1 and 2 in the partition i.

[1]Strictly speaking, the overlap of the Borromean ^{6}He wave function with the wave function of the particle-unstable nucleus ^{5}He does not necessarily lead to the single-particle wave function whose asymptotic is defined by the neutron separation energy. Since, however, we consider only two-body channels in our CRC approach, we still use the separation energy prescription for the $\langle ^6\mathrm{He}|^5\mathrm{He}\rangle$ overlap keeping in mind that accuracy of this approximation should be investigated separately in the future.

TABLE I. Spectroscopic amplitudes A_{lsj} used in the coupled channel calculations.

	lsj	A_{lsj}
$t=d\otimes n$	$0\,\frac{1}{2}\,\frac{1}{2}$	-1.225
$^5\mathrm{He}(3/2^-)={}^4\mathrm{He}\otimes n$	$1\,\frac{1}{2}\,\frac{3}{2}$	-1.118
$^6\mathrm{He}={}^5\mathrm{He}(3/2^-)\otimes n$	$1\,\frac{1}{2}\,\frac{3}{2}$	1.4365
$^6\mathrm{Li}(1^+)={}^5\mathrm{He}(3/2^-)\otimes p$	$1\,\frac{1}{2}\,\frac{3}{2}$	0.7322
$^6\mathrm{Li}(1^+)={}^5\mathrm{He}(3/2^-)\otimes p$	$1\,\frac{1}{2}\,\frac{1}{2}$	0.5598
$^6\mathrm{Li}(3^+)={}^5\mathrm{He}(3/2^-)\otimes p$	$1\,\frac{1}{2}\,\frac{3}{2}$	-1.0954
$^6\mathrm{Li}(1^+)={}^4\mathrm{He}\otimes d$	0 1 1	-1.056
$^6\mathrm{Li}(3^+)={}^4\mathrm{He}\otimes d$	0 2 3	1.0607

The charge-exchange form factor $\langle ^6\mathrm{He}|^6\mathrm{Li}(1^+)\rangle$ has been taken from [2]. However, here we keep only the $l=0$ part of the transition density. We have neglected the charge-exchange coupling between the $p+{}^6\mathrm{He}$ and $n+{}^6\mathrm{Li}(3^+)$ channel because it is determined by a weak $l=2$ transition.

The full finite-range treatment of one- and two-nucleon transfer form factors has been performed including the remnant term in the transition operator and the nonorthogonality corrections. The inclusion of the nonorthogonality terms is crucial to get the same coupled-channels results both in post and prior forms of coupling terms. We do observe a good agreement between the post and prior calculations when only one-body couplings are present, However, the choice between post and prior representations for the two-nucleon transfer form factor still produces 5–20 % difference in the angular distributions but no more than 5% change in the total cross sections. This difference is much smaller than the uncertainty arising due to the choice of the input interactions and wave functions.

First of all, in order to see the relative importance of different couplings in the $p+{}^6$He scattering at the chosen energy, we have performed several preliminary coupled channel calculations where only some selected channels or couplings have been retained with the model A being used for the ^{6}He nucleus at this stage. For example, three mechanisms may be responsible for the population of the $^4\mathrm{He}+t$ channel: direct transfer (p,t) of two nucleons, two step transfer $(p,d)(d,t)$ and two step exchange-transfer $(p,n)(n,t)$. So, we have performed three coupled channel calculations with zero imaginary parts keeping only: (i) partitions I, IV and two-neutron transfer form factor; (ii) partitions I, II, IV and one-nucleon transfer form factors; (iii) partitions I, IIIa, IV, charge exchange and deuteron transfer form factors. Two-way couplings were always considered, with their effects included to all orders in the CRC solution. The results are presented in Fig. 2 where they are compared with full CRC calculations. One can see that the simultaneous transfer (p,t) and two-step $(p,n)(n,t)$ mechanisms give similar shapes for the angular distributions of the $^6\mathrm{He}(p,t)^4\mathrm{He}$ reaction, which are very different from the two-step $(p,d)(d,t)$ transfer via the $^5\mathrm{He}(3/2^-)$ resonance. The angular distributions obtained from the full CRC calculations are similar to those calculated assuming only the $(p,d)(d,t)$ couplings but the absolute values of the full CRC

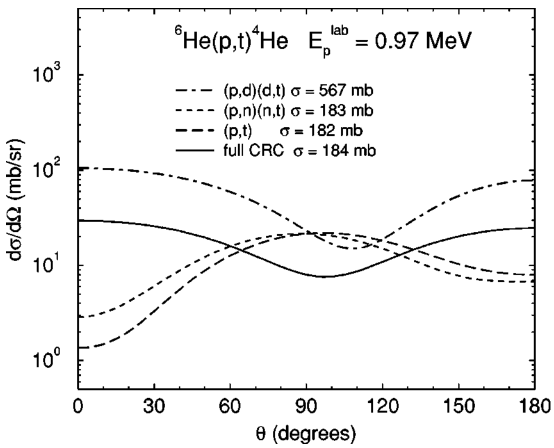

FIG. 2. Coupled channel calculations of the ^{6}He$(p,t)^4$He reaction restricted to two-neutron transfer (dashed line), sequential $(p,d)(d,t)$ transfer (dotted-dashed line) and two-step $(p,n)(n,t)$ exchange-transfer (dotted line). Full CRC calculations are presented by solid line. See text for details.

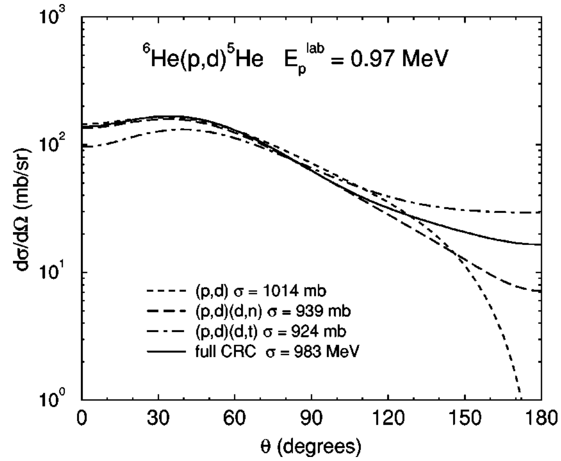

FIG. 4. The ^{6}He$(p,d)^5$He reaction obtained from couplings only between proton and deuteron channels (dotted line), from reaction paths $(p,d)(d,n)$ (dashed line) and $(p,d)(d,t)$ (dotted-dashed line). Full CRC calculations are presented by solid line. See text for details.

cross section are about three times smaller.

Another example is the population of the $n+{}^6$Li(g.s.) channel which may proceed either directly by (p,n) charge exchange or via the two-step $(p,d)(d,n)$ transfer. So, we have performed two calculations keeping only (i) partitions I, IIIa and charge-exchange form factor and (ii) partitions I, II, IIIa, and one-nucleon transfer form factors. The results are presented in Fig. 3. The population of the same channel $n+{}^6$Li can also be calculated as an intermediate stage of a CRC calculation with bidirection charge exchange-transfer $(p,n)(n,t)$ couplings to the ^{4}He$+t$ channel. The cross sections of the (p,n) reactions obtained from the previous $(p,n)(n,t)$ calculations and full CRC calculations are shown in Fig. 3 as well. Figure 3 shows that the (p,n) and $(p,d)(d,n)$ paths generate large ^{6}He$(p,n)^6$Li cross sections, but as soon as the large-Q-value channel ^{4}He$+t$ is open, the (p,n) cross sections drop significantly. We do not show the results for the ^{6}He$(p,n)^6$Li(3^+) reaction since we did not take into account $l=2$ exchange form factor which is important for this particular channel. These cross sections are small, more sensitive to the errors of calculations and therefore less reliable.

In all the examples considered above there is flux transfer to the $d+{}^5$He channel. The cross sections of the ^{6}He$(p,d)^5$He reaction corresponding to different combinations of reaction paths, as well as to full CRC calculations, are shown in Fig. 4. One can conclude that the shape of the angular distribution is almost independent of the coupling scheme chosen. The absolute values of these cross sections are very close to those calculated assuming only (p,d) or $(p,d)(d,n)$ paths.

Each variant of the coupling scheme considered above produces angular distributions of the elastic scattering $p+{}^6$He. Elastic scattering calculated with partitions (i) I, II, IIIa;

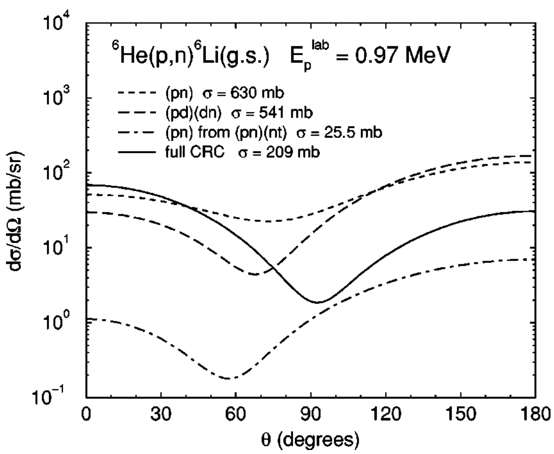

FIG. 3. Coupled channel calculations of the ^{6}He$(p,n)^6$Li(g.s.) reaction restricted to charge exchange only (dotted line), sequential $(p,d)(d,n)$ transfer (dashed line) and two-step $(p,n)(n,t)$ exchange-transfer (dashed-dotted line). Full CRC calculations are presented by solid line. See text for details.

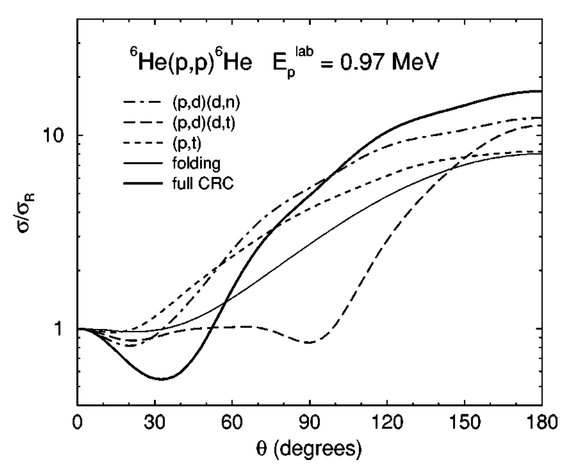

FIG. 5. Elastic-scattering ratio to Rutherford for ^{6}He$(p,p)^6$He arising in different coupling schemes, in no-absorption optical model (thin solid line) and full CRC calculations (thick solid line). See text for details.

(ii) I, II, IV, and (iii) I, IV are compared in Fig. 5 to the elastic scattering calculated in the no absorption optical model with the same folding potential. The angular distributions calculated with partitions (iv) I, IIIa, IV are not distinguishable from case (iii) therefore they are not shown in Fig. 5. The (p,t) and $(p,n)(n,t)$ coupling schemes gave the smallest deviation of the elastic scattering angular distributions from the no-absorption folding optical model. The deviation is larger for the $(p,d)(d,n)$ and $(p,d)(d,t)$ reaction paths, however, their influence is very different. The full CRC elastic-scattering angular distributions deviate from the no-absorption optical model most strongly.

Partial cross sections for deuteron, triton, and neutron final channels are presented in Fig. 6. Strong contributions from the $1/2^+$ partial wave can be seen in this figure which is naturally expected for the very low projectile energies. However, significant increase of the cross sections in the $3/2^-$ partial wave witnesses the presence of the resonance in this wave. Such a resonance indeed exists in the spectrum of the ^{7}Li nucleus at 9.9 MeV and has a large width of 1.2 MeV.

The resulting cross sections for all channels depend strongly on the input parameters, mainly on the signs and values of spectroscopic amplitudes and three-body wave function of ^{6}He. Studies of single nucleon transfer reactions on $1p$-shell nuclei have shown many times that, in general, the shell model spectroscopic factors are quite reliable. Therefore, we will show how the choice of the model for the three-body ^{6}He wave function influences the cross sections in the CRC calculations. We repeated the full CRC calculations with the three-body ^{6}He wave function B with shorter radius three-body force, and hence the smaller root-mean-square matter radius for ^{6}He of 2.35 fm. We have found out that if different models of ^{6}He are used to calculate the $p-{}^6$He folding potential, the results are not sensitive to that choice. However, different ^{6}He wave functions used for the two-nucleon transfer form factor give dramatic changes to the results of the CRC calculations, which are demonstrated by Fig. 7. One can see that angular distributions have been changed significantly, especially for the deuteron output

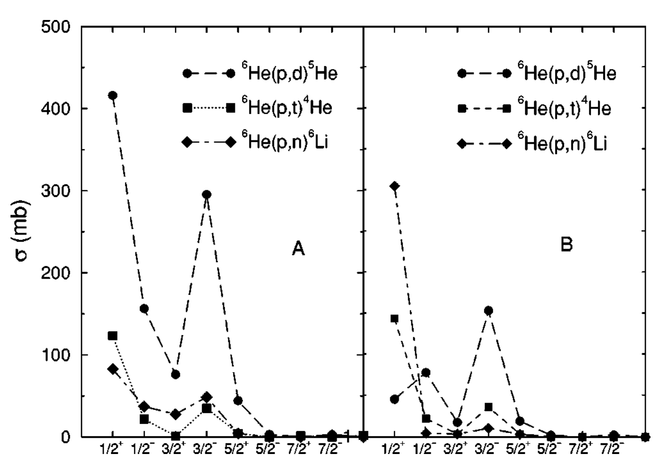

FIG. 6. Partial cross sections for the ^{6}He$(p,d)^5$He, ^{6}He$(p,t)^4$He and ^{6}He$(p,n)^6$Li reactions calculated in the full CRC, for different ^{6}He models A and B which predict ^{6}He r.m.s. radii of 2.50 and 2.35 fm, respectively.

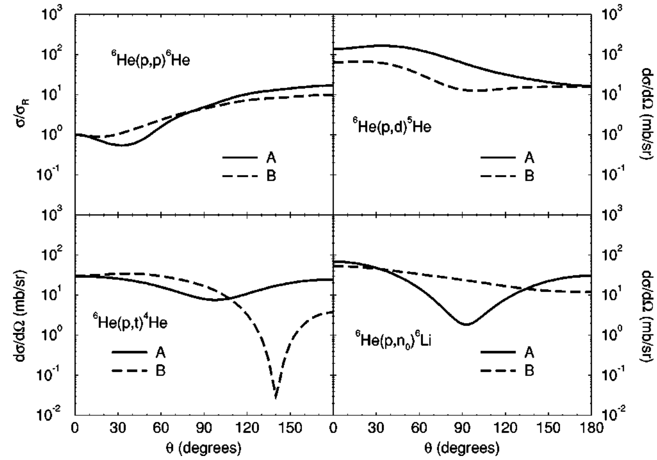

FIG. 7. Full CRC cross sections calculated with the two-neutron transfer form factor corresponding to the large ^{6}He model A and the smaller model B with r.m.s. radii of 2.50 and 2.35 fm, respectively.

channel. Total cross section of the (p,d) reaction has decreased by a factor of 3 (see Table II), slightly increased for (p,t) reactions and increased by 50% for the (p,n_0) reactions. Total reaction cross section has decreased by 37%. Thus, it shows that the simultaneous two-nucleon transfer at low energies does play an important role in formation of the distribution of the incident flux into different final channels. Simultaneous experimental studies of proton-induced reactions on ^{6}He at low energies can therefore help to understand better the structure of the three-body function of ^{6}He.

III. EXCHANGE EFFECTS

There are two groups of exchange effects in the $p+{}^6$He scattering. One of them involves all possible transfers of heavy particles, for example, ^{6}He$(p,{}^6$Li$)n$, ^{6}Li$(n,{}^5$He$)d$, etc., and another one includes all possible rearrangements within the α core itself. In the previous sections only direct mechanisms were considered. However there are cases, considered in [16] for example, where the exchange effects may play an important role at low energies as well.

Our DWBA estimations show that the contribution of the exchange effects of the first kind is about 5 to 6 orders of magnitude smaller than that from the direct transfers. In our case the most significant exchange effect of the second kind may arise due to the presence of the $t+t$ configuration in

TABLE II. Reaction cross sections calculated with different two-neutron transfer form factors corresponding to different models A and B for the ^{6}He g.s., with different radii.

Reaction	σ_R (mb) A: $\langle r^2\rangle^{1/2}=2.50$ fm	B: $\langle r^2\rangle^{1/2}=2.35$ fm
(p,d)	983	321
(p,t)	184	212
(p,n_0)	209	328
(p,n_1)	35	22
Total	1411	883

TABLE III. Effective optical model potential which reproduce the elastic scatterings from the full coupled channel calculations. The potential depths and laboratory energies are in MeV, radii and diffusenesses are in fm and $R_i = r_i A_T^{1/3}$. See text for the spin-orbit interaction in the $t+{}^4$He channel.

	$E_{\rm lab}$	V_R	r_R	a_R	W_D	r_D	a_D
$p+{}^6$He	0.97	49.35	1.33	0.155	17.83	1.804	0.161
$d+{}^5$He	1.66	101.63	2.728	0.199	26.15	2.207	0.0483
$t+{}^4$He	14.59	105.9	1.98	0.405	29.8	1.91	0.045

^{6}He. It is well known that this configuration is important to obtain a correct binding energy of ^{6}He in the resonating group method [17]. The $^6\text{He}=t+t$ configuration has been already experimentally investigated in the ^{7}Li$(t,{}^6\text{He})^4$He, ^{19}F$(t,{}^6\text{He})^{16}$O, ^{13}C$(t,{}^6\text{He})^{10}$B, and ^{12}C$(t,{}^6\text{He})^9$B triton transfer reactions at $E_t=38$ MeV [18]. In that work the description of the angular distributions of the ^{13}C$(t,{}^6\text{He})^{10}$B and ^{12}C$(t,{}^6\text{He})^9$B reactions was very poor and therefore these reactions can not serve as a source of the reliable determination of the spectroscopic factors. The description of the angular distribution of the ^{7}Li$(t,{}^6\text{He})^4$He reactions was good in the angle range available from the experiment. However, in this case an important contribution from the remnant term of the transition operator should arise. Neither this contribution nor an interference with the exchange ^{7}Li$(t,{}^4\text{He})^6$He mechanism had been taken into account and therefore the spectroscopic information from this reaction was not reliable. As for the ^{19}F$(t,{}^6\text{He})^{16}$O reaction, the description of its angular distribution was very satisfactory and the extracted spectroscopic factors do not contradict to the theoretical shell-model value of -1.33 for the spectroscopic amplitude for the $\langle {}^6\text{He}|t\otimes t\rangle$ overlap.

At present we are not able to include exchange effects in the coupled reaction channel scheme. So, we estimate the role of the ^{6}He$(p,{}^4\text{He})t$ exchange transfer in the DWBA. To provide necessary optical potentials, we first fit the angular distributions for $p+{}^6$He, $d+{}^5$He, and $^4\text{He}+t$ elastic scatterings calculated in Sec. II. The effective optical potentials are presented in Table III. While we succeeded to reproduce the $p+{}^6$He and $d+{}^5$He elastic scatterings only with central optical potentials, the introduction of the spin-orbit potential with $V_{\rm so}=4.6$ MeV, $r_{\rm so}=1.97$ fm, and $a_{\rm so}=0.29$ fm was necessary to describe the $t+{}^4$He elastic scattering. The central potentials are presented in Table III. The angular distributions calculated within the full CRC, and their optical model fit, are shown in Fig. 8.

To calculate the ^{6}He$(p,{}^4\text{He})t$ reactions, we used a two-body potential model for the $t+t$ bound-state wave function with $r_0=0.66$ fm and $a=0.65$ fm without spin-orbit interaction, assuming $R=r_0(A_1^{1/3}+A_2^{1/3})$. As in [18], we use the spectroscopic amplitude for the $\langle {}^6\text{He}|t\otimes t\rangle$ overlap equal to -1.33. The full transition operator has been used and the agreement between the post and prior forms has been achieved. The calculated ^{6}He$(p,{}^4\text{He})t$ angular distributions are compared in Fig. 9 with direct one-step (p,t) transfer obtained with the same optical potentials and with model A

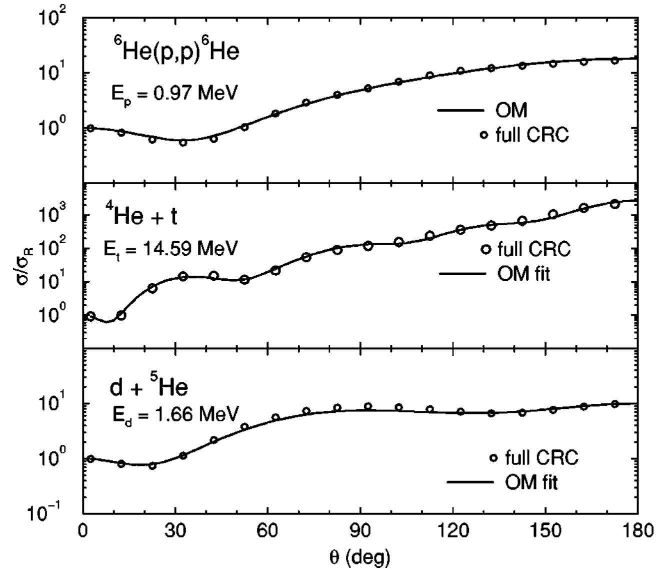

FIG. 8. Angular distributions of the elastic scatterings in the $p+{}^6$He, $t+{}^4$He, and $d+{}^5$He channels obtained in full coupled channel calculations and their optical model fits.

for the ^{6}He wave function in the DWBA. One can see that, within the DWBA, the triton exchange transfer leads to much larger cross sections than the direct two-neutron transfer.

As for the sequential $(p,d)(d,t)$ transfer, it is not possible to separate uniquely its contribution due to nonorthogonality considerations [19]. We show in Fig. 9 the results of the prior-post calculations of the ^{6}He$(p,d)(d,t)^4$He in which the contribution of the nonorthogonality term is zero. The DWBA two-step transfer cross sections are much larger than the DWBA one-step (p,t) cross sections. This result could lead to the conclusion that the role of the simultaneous two-neutron transfer is small at very low energies. However, as

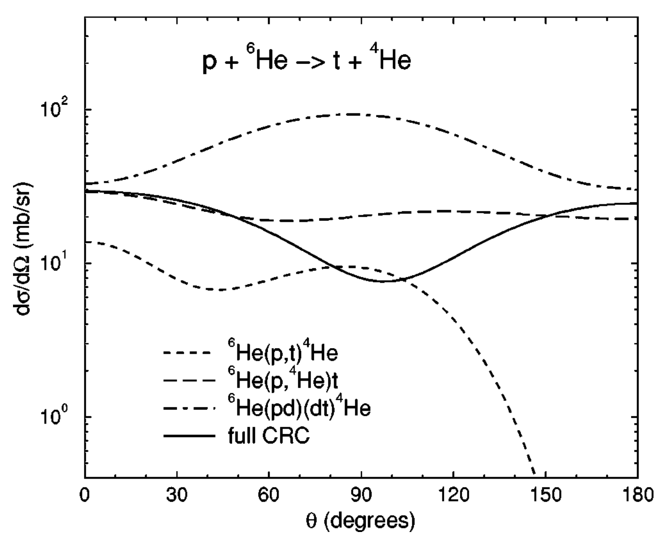

FIG. 9. The DWBA calculations of the exchange triton transfer ^{6}He$(p,{}^4\text{He})t$ (dashed line), simultaneous two-neutron transfer (short dashed line) and sequential $(p,d)(d,t)$ transfer (dashed-dotted line). The results of the full CRC calculations from Sec. II are shown by a solid line for comparison.

we have shown in our previous section, the two-neutron transfer does play an important role in the full CRC calculations. Neglecting or varying the (p,t) coupling in the CRC scheme leads to significant change of cross sections in all final channels. The DWBA angular distribution in the final ^{4}He$+t$ channel differs by its shape from those obtained in the CRC calculations. Thus the conclusion about the relative contribution of the simultaneous and sequential two-neutron transfer within the framework of the DWBA may be misleading.

The ^{6}He$(p,{}^4$He$)t$ cross sections are comparable to the full CRC (p,t) cross sections. This means that the inclusion of the exchange triton transfer into the coupling scheme may also significantly influence the distribution of the incident proton flux into all final channels.

IV. RADIATIVE CAPTURE

There should be a qualitative difference between the radiative proton capture by proton-rich nuclei and the radiative proton capture by neutron-rich nuclei at the low energies. In the former case the proton capture is strongly influenced by the long tail of the bound-state wave function of the captured proton and the proton-nuclear potential has only a secondary effect on the capture cross sections while in the later case the separation energy of the captured proton is normally very large and its wave function is mainly concentrated inside the nuclear interior thus making the cross sections to be more model dependent. In addition, proton emission thresholds are very different for the systems composed by proton-rich nucleus + proton and neutron-rich nucleus + proton. Being very high for the neutron-rich nuclei, they often lie above other particle emission thresholds so that the proton-nucleus interaction cannot be chosen to be real anymore. The absorption from elastic channel to other channels may lead to the suppression of the continuum wave function in the internal part in nucleus and therefore to the decrease of the proton capture cross sections.

In the particular case of ^{6}He$+p$ the separation energy of the captured proton in the residual nucleus ^{7}Li is 9.9 MeV. Therefore, the contribution of the tail of its wave function to the capture amplitude should be reduced. On the other hand, the continuum $p+{}^6$He wave function has a node in the s wave because of the Pauli principle. Therefore, an interference between the internal and external amplitudes takes place, which makes the cross sections even smaller. Since the Coulomb barrier in the case of the $p+{}^6$He is very low, the proton penetrates inside the nucleus and the continuum proton wave function should be sensitive to the interaction potential between proton and ^{6}He. Different interaction potentials will give different cancellations between external and internal parts of the transition amplitude, thus showing an enchanced sensitivity of the calculated capture cross sections to the p-^{6}He potential. Finally, the proton emission threshold in ^{7}Li lies above three other thresholds, so that transitions to other reaction channels are open and the $p+{}^6$He interaction potential must contain imaginary part. Therefore, the cross sections of the ^{6}He$(p,\gamma)^7$Li radiative capture should be further reduced due to the absorption effects.

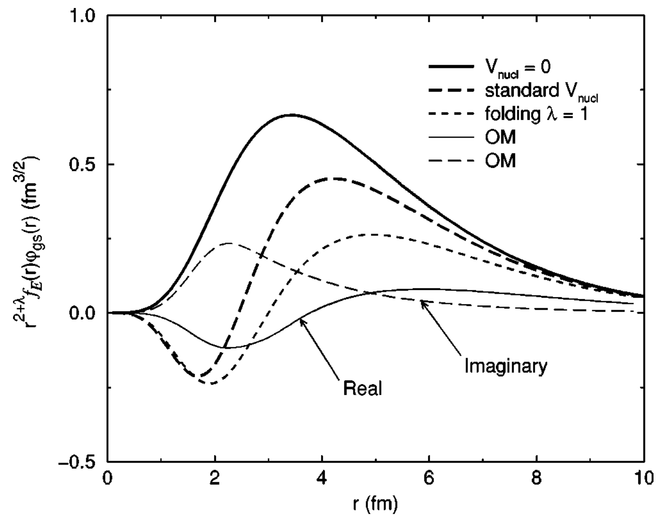

FIG. 10. The integrand of the $E1$ transition amplitude for the ^{6}He$(p,\gamma)^7$Li(g.s.) reaction at $E_p=0.97$ MeV calculated with different potentials of the p-^{6}He interaction in the incident channel.

To illustrate all that was said above, we have plotted in Fig. 10 the integrand $r^3 f_E(r)\varphi_{gs}(r)$ of the $E1$ transition amplitude for the ^{6}He$(p,\gamma)^7$Li(gs) reaction at $E_p=0.97$ MeV. A two-body potential model with standard geometry parameters $r_0=1.25$ fm $a=0.65$ fm and without spin orbit potential was used to calculate the $p+{}^6$He bound-state wave function, with the depth of the $p+{}^6$He potential chosen to reproduce the proton separation energy in ^{7}Li. The spectroscopic factor for the $\langle {}^7\mathrm{Li}|{}^6\mathrm{He}\otimes p\rangle$ overlap equal to 0.3 [20] was used to normalize the final cross section. With fixed bound-state wave function, different variants of the $p+{}^6$He continuum potentials have been used: (i) only Coulomb potential, (ii) Coulomb plus standard nuclear potential of $V=50$ MeV, $r_0=1.25$ fm, and $a=0.65$ fm, (iii) Coulomb plus folded $p+{}^6$He potential and (iv) Coulomb plus

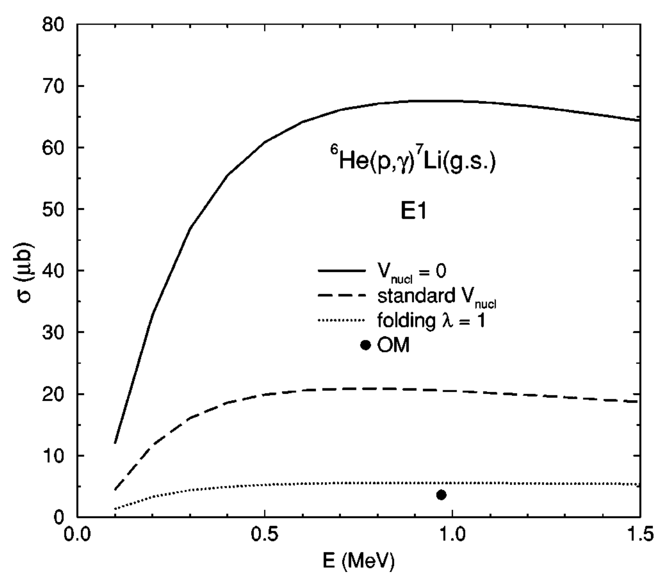

FIG. 11. $E1$ cross sections for the ^{6}He$(p,\gamma)^7$Li(g.s.) reaction calculated with different potentials of the p-^{6}He interaction in the incident channel.

effective complex optical potential from Table III derived in Sec. III. One can see that in the absence of the nuclear force, the integrand does not have any nodes. As the nuclear force is switched on, the node in the scattering state wave function appears and the maximum values of the integrand significantly decrease. This will lead to the cancellation between internal and external contributions to the transition amplitude which are different for different choice of the nuclear potential. The effective optical potential leads to absorption from the incident channel and it pushes slightly the scattering state wave function from the nuclear interior, as well as decreasing its absolute value. The contribution from the imaginary part of the distorted-wave function is concentrated close to the nuclear surface and it will correspond to the effects on the radiative capture of other open channels to which some of the incident flux has escaped.

The calculated $E1$ cross sections are presented in Fig. 11. One can see that in the absence of nuclear interaction in the incident channel the cross sections are large. Nuclear interaction strongly reduces this cross section. Optical model treatment of the incident p-^{6}He motion leads to a small cross section $\sigma=3.6\ \mu$b. The inclusion of other multipoles will not dramatically change this estimation. The estimated cross section of the (p,γ) reaction is about five orders of magnitude smaller than the reaction cross section caused by strong interaction. This justifies noninclusion of the ^{7}Li$+\gamma$ channel in the coupling scheme used to describe proton-induced scattering on ^{6}He.

V. CONCLUSION

We have performed a finite-range CRC calculations of the $p+{}^6$He scattering at $E_p^{\rm lab}=0.97$ MeV assuming that the α-particle core is inert. The choice of the incident proton energy has been made to avoid the complications due to the ^{6}He breakup and the transition to the superallowed ^{6}Li$(0^+;1)+n$ channel. Furthermore, this energy is available at the Louvain-la-Neuve cyclotron, where preliminary measurements for (p,t) reaction at a similar energy have already been performed.

The calculations have revealed a complicated dynamics of the $p+{}^6$He interaction at this energy. Couplings to all open channels were important to generate the final cross sections. The total absorption from the elastic $p+{}^6$He channel depends on the details of the interactions employed in the three-body model of ^{6}He and shows a strong correlation with the r.m.s. radius of ^{6}He. The radius of 2.50 fm has given the total absorption of 1411 mb, while a smaller radius of 2.35 fm has given much smaller absorption of 883 mb (see Table II). In the case of larger radius the main absorption was due to the (p,d) reaction with $\sigma_R=983$ mb, while the (p,t) and (p,n) reactions had comparable cross sections to each other. In the case of smaller radius the total absorption was more uniformly distributed between the (p,d), (p,t), and (p,n) channels (Table II). The strong decrease of the (p,d) cross sections is related with dramatic redistribution of the $1/2^+$ partial cross sections between different reaction channels (see Fig. 6). Such a redistribution should make us to able to discriminate between the models describing ^{6}He. However, this discrimination can take place only after inclusion of the exchange triton transfer into the coupling scheme.

The cross sections of the (p,t) reaction calculated in our paper with any choice of the input parameters are about three orders of magnitude larger than those predicted in Ref. [4]. Unfortunately, we cannot comment on the reason for this discrepancy because the physical parameters of their DWBA calculations are not given.

In conclusion, the investigation of ^{6}He-induced reactions on a hydrogen target may help us to learn more about the structure of the halo nucleus ^{6}He. Therefore, further experimental investigation of these reactions started in [1] would be very interesting.

ACKNOWLEDGMENTS

We are grateful to S.N. Ershov for providing us with numerical values of the $\langle {}^6\mathrm{He}|{}^6\mathrm{Li}\rangle$ transition densities, and L. Grigorenko for constructive comments. Support from EPSRC Grant No. GR/J/95867 is acknowledged.

[1] A. N. Ostrowski *et al.*, J. Phys. G **24**, 1553 (1998).
[2] S. N. Ershov *et al.*, Phys. Rev. C **56**, 1483 (1997).
[3] M. V. Zhukov, B. V. Danilin, D. V. Fedorov, J. M. Bang, I. J. Thompson, and J. S. Vaagen, Phys. Rep. **231**, 151 (1993).
[4] H. Lenske and G. Schrieder, Eur. Phys. J. A **2**, 41 (1998).
[5] D. V. Aleksandrov, E. Yu. Nikol'skii, B. G. Novatskii, and D. N. Denisov, Pis'ma Zh. Éksp. Teor. **59**, 301 (1994) [JETP Lett. **59**, 320 (1994)].
[6] Yu. Ts. Oganessian, V. I. Zagrebaev, and J. S. Vaagen, Phys. Rev. Lett. **82**, 4996 (1999).
[7] I. J. Thompson, Comput. Phys. Rep. **7**, 167 (1988).
[8] B. V. Danilin, I. J. Thompson, J. S. Vaagen, and M. V. Zhukov, Nucl. Phys. **A632**, 383 (1998).
[9] J. Bang and C. Gignoux, Nucl. Phys. **A313**, 119 (1979).
[10] D. Gogny, P. Pires, and R. de Tourreil, Phys. Lett. **32B**, 591 (1970).
[11] P. Banerjee, J. A. Tostevin, and I. J. Thompson, Phys. Rev. C **58**, 1337 (1998).
[12] G. Bertsch, J. Borysowicz, H. McManus, and W. G. Love, Nucl. Phys. **A284**, 399 (1977).
[13] C. W. De Jafer, H. de Vries, and C. de Vries, At. Data Nucl. Data Tables **14**, 479 (1974).
[14] Yu. M. Tchuvil'skii and Yu. F. Smirnov, Phys. Rev. C **15**, 84 (1977).
[15] A.N. Boyarkina, *Structure of* 1*p-shell nuclei* [in Russian] (Moscow State University, Moscow, 1973).
[16] Y. Yamashita, Nucl. Phys. **A582**, 270 (1995); Y. Yamashita and Y. Kudo, Prog. Theor. Phys. **90**, 1303 (1993).
[17] A. Csótó, Phys. Rev. C **48**, 165 (1993).
[18] N. M. Clarke, J. Phys. G **18**, 917 (1992).
[19] G. R. Satchler, *Direct Reaction Theories* (Oxford Press, New York, 1983).
[20] S. Cohen and D. Kurath, Nucl. Phys. **101**, 1 (1967).